Over-winter persistence of supraglacial lakes on the Greenland Ice Sheet: results and insights from a new model

Robert Law[1], Neil Arnold[1], Corinne Benedek[1], Marco Tedesco[2,3], Alison Banwell[4,1] 🆔 and Ian Willis[1] 🆔

[1]Scott Polar Research Institute, University of Cambridge, UK; [2]Lamont-Doherty Earth Observatory of Columbia University, New York City, NY, USA; [3]NASA Goddard Institute of Space Studies, New York City, NY, USA and [4]Cooperative Institute for Research in Environmental Sciences, University of Colorado Boulder, CO, USA

Abstract

We present a newly developed 1-D numerical energy-balance and phase transition supraglacial lake model: GlacierLake. GlacierLake incorporates snowfall, in situ snow and ice melt, incoming water from the surrounding catchment, ice lid formation, basal freeze-up and thermal stratification. Snow cover and temperature are varied to test lake development through winter and the maximum lid thickness is recorded. Average wintertime temperatures of -2 to $-30°C$ and total snowfall of 0 to 3.45 m lead to a range of the maximum lid thickness from 1.2 to 2.8 m after ∼250 days, with snow cover exerting the dominant control. An initial ice temperature of $-15°C$ with simulated advection of cold ice from upstream results in 0.6 m of basal freeze-up. This suggests that lakes with water depths above 1.3 to 3.4 m (dependent on winter snowfall and temperature) upon lid formation will persist through winter. These buried lakes can provide a sizeable water store at the start of the melt season, expedite future lake formation and warm underlying ice even in winter.

Introduction

Mass loss from the Greenland Ice Sheet (GrIS) has significantly accelerated during the last several decades to become a major cryospheric contributor to global sea-level rise (Rignot and others, 2011; Jacob and others, 2012; The IMBIE Team, 2019). Since 1991, 60% of GrIS mass loss has been attributed to surface meltwater runoff (van den Broeke and others, 2016), with total meltwater set to increase over the 21st century as Arctic warming accelerates (AMAP, 2017), the capacity of firn to refreeze percolating meltwater decreases (De La Peña and others, 2015; Mikkelsen and others, 2016; Noël and others, 2017; Steger and others, 2017) and the equilibrium line altitude moves inland (Leeson and others, 2015). These figures all emphasise the importance of developing a holistic understanding of the GrIS supraglacial hydrology system (Rennermalm and others, 2013).

Research on supraglacial lakes, which are one component of the supraglacial hydrology system, has advanced rapidly during the last decade (Chu, 2014; Nienow and others, 2017). However, the ways in which future warming will influence the lakes' spatial and temporal patterns (Box and Ski, 2007; McMillan and others, 2007; Liang and others, 2012; Johansson and others, 2013; Fitzpatrick and others, 2014) and the surface-to-bed linkages for which they are frequently responsible (Das and others, 2008; Hoffman and others, 2018), remain poorly constrained (Mayaud and others, 2014; Banwell and others, 2016; Koziol and others, 2017), and are gaining importance as supraglacial lakes are observed to be present over increasing portions of the ice sheet (Leeson and others, 2015; Gledhill and Williamson, 2017; Williamson and others, 2018a).

Greenland's supraglacial lakes can transiently occupy ∼2.7% of the ablation zone (Box and Ski, 2007) and form in the same locations year-on-year as a result of ice surface expression of basal topography (Echelmeyer and others, 1991; Lampkin and VanderBerg, 2011). The lakes are observed to drain, either rapidly down hydro-fractured moulins (Das and others, 2008; Doyle and others, 2013) (∼10% of lakes; Selmes and others, 2013), or more gradually by over topping and incising their catchment (Tedesco and others, 2013) (∼50% of lakes; Selmes and others, 2013). The precise conditions that cause some, but not all, lakes to drain through hydrofracture remain elusive (Williamson and others, 2018b), though the overall effect of rapid lake drainage on ice velocity in land-terminating sectors of the GrIS is not as great as initially thought (Nienow and others, 2017). The moulins they frequently open however, do exert long-lasting control on the subglacial hydrology system (Banwell and others, 2016; Koziol and others, 2017; Williamson and others, 2018a). Many authors interested in supraglacial lake processes and effects assume that the ∼40% of lakes that remain in situ at the end of the melt season (Selmes and others, 2013) either freeze entirely in winter (Johansson and others, 2013; Selmes and others, 2013; Koziol and others, 2017), or freeze partially and play no future rule in the hydrology of the GrIS (Arnold and others, 2014). This view is supported in remote sensing from Miles and others (2017) who suggest full winter freezing

of lakes based on C-band Sentinel-1 satellite data, although they acknowledge this conclusion may be a result of the low penetration of the C-band radar (1–2 m).

Conversely Koenig and others (2015) use L-band IceBridge airborne radar data to observe winter 'buried lakes' (sometimes called 'subsurface lakes') containing liquid water across the entire periphery of the GrIS, in the same location as MODIS detected summer lakes. These buried lakes are not normally observable from surface topography, although radar data shows an average overlying snow-depth of 0.65 m and an ice-lid thickness of 1.4 m (both are influenced by the timing of IceBridge flights). Russell (1993) also infers the presence of buried lakes from ice-sheet marginal meltwater release near Kangerlussuaq, concurrent with the development of two circular depressions where lakes had previously been observed 20–30 km inland. The first order estimate of 1.5 Gt of water accumulated in buried lakes (Koenig and others, 2015) is small in comparison with the 140 Gt believed to be in firn aquifers (Forster and others, 2014), or the 100–300 Gt of melt lost through GrIS annual surface melt (Vernon and others, 2013). Nevertheless, a buried lake acts as a 0°C boundary whenever it is present, warming underlying ice even as a surface energy input decreases in winter, with potential implications for ice rheology and therefore fracture mechanics. A buried lake also acts as a store of water that may expedite the subsequent summer evolution of the supraglacial hydrological system. The thermal signature of lakes is important in cryo-hydrologic warming (Phillips and others, 2010, 2013) as another way to warm the near-surface ice sheet, and for temperature analysis where surface features are found to exert a strong influence on temperature profiles (Catania and Neumann, 2010; Lüthi and others, 2015; Hills and others, 2017). These studies emphasise the need for a physically based and rigorous analysis of multi-year supraglacial lake evolution to provide better information for GrIS hydrology studies on the fate, and thermal effects, of lakes following the end of the summer melt season.

Here, a numerical modelling approach is used to gain a detailed understanding of the evolution of supraglacial lakes. GlacierLake is presented: an efficient and realistic model of supraglacial lake evolution, applicable across the ablation zone of any glacier (though modifications may be required for debris covered glaciers), but used here to investigate lake evolution on the GrIS. GlacierLake completes a year-long run in half a minute on a 3.2 GHz processor. This allows for GlacierLake's use across large areas, and allows coupling with broader hydrological models if required (e.g. Koziol and Arnold, 2018). A fast run-time also enables extensive sensitivity testing which adds to the reliability and transparency of model results.

Existing models

Numerical models of snow, and of lakes underlain by ice or permafrost have been developed and applied over the last two decades. The earliest relevant model is from Ebert and Curry (1993) who focused on meltwater lake formation atop sea ice, based on original equations by Maykut and Untersteiner (1971). Sea ice lake models improved over the decades (Morassutti and Ledrew, 1996; Fetterer and Untersteiner, 1998; Taylor and Feltham, 2004; Skyllingstad and others, 2009) culminating in work by Scott and Feltham (2010), who produced a fully 3-dimensional lake evolution model for first-year and multi-year sea ice. The terrestrial MyLake model of Saloranta and Andersen (2007), originally developed for phosphorous-phytoplankton dynamics, performs well for temperature and ice lid thickness modelling, with a rapid run time. However the exclusion of a lower, spatially flexible phase boundary and underlying glacier-ice section means

basal freeze-up and its effects on underlying temperature profiles cannot be constrained.

Models to simulate the evolution of supraglacial lakes began with Lüthje and others (2006) who derive their analysis from Ebert and Curry (1993) and use the explicit heat equation discretisation from Alexiades and Solomon (1993). Lüthje and others (2006) examined the abundance of supraglacial lakes in satellite imagery and combined this with the use of a 1-D model to examine the effects of a meltwater column on energy transfer, finding that the basal ablation of lakes is 110–170% that of the immediate surrounding bare ice. Benedek (2014) used code from Lüthje and others (2006) to extend the length of the shortwave radiation path from the lake surface to the bed, based on refraction at the lake surface. Benedek (2014) found this caused relatively little change to the overall evolution of the lakes, with parameter uncertainty (such as surface absorption of shortwave radiation) having a greater influence. The models of Lüthje and others (2006), Tedesco and others (2012) and Benedek (2014) were run for no longer than 30 days, and lid formation, allowance for a transition from bare ice to water, and lid collapse, were not incorporated. The explicit discretisation of these models means the time step was held below 6 min to avoid numerical instability, resulting in greater computational expense than with an implicit scheme. Lastly, Buzzard and others (2018) present currently the most physically comprehensive lake model, developed for ice shelves in Antarctica where firn compaction, saturation and refreezing are important. However, detailed modelling of these aspects increases the run-time of the model from minutes to hours and is not required when the lake forms atop solid ice following early snowmelt.

Model development

Model architecture

GlacierLake was written in MATLAB R2017b using the equations presented below, with source code and equations adapted from Benedek (2014) (who adapted source code from Lüthje and others, 2006), Buzzard and others (2018), Saloranta and Andersen (2007) and Essery (2015). GlacierLake represents a single point in x, y space modelled as a $1 \, \text{m}^2$ column as any scaling factors cancel. The model is divided into five stages (Fig. 1 and Table 1). Movement through GlacierLake, and processes at each stage, are detailed in Table 2 and occur once a given threshold has been reached. The model is also allowed to move backwards through stages (for example stage 5 to 3 in Fig. 1) to mimic year-on-year evolution. The model was developed using weather data from the Program for Monitoring of the GrIS (PROMICE, vanAs and others, 2010). The AWS UPE-U, at an elevation of 980 m a.s.l. and 72.89°N, 53.58°W, was used for development, as the record for this station was the most comprehensive of any PROMICE station in the ablation zone of the GrIS.

GlacierLake comprises two modules. The main module contains cells of constant size throughout the model run (default 0.1 m for upper 15 m and, 1 m below). These cells are in one of three states: ice, water or 'slush', where ice and water coexist in a ratio dependent upon the total enthalpy of the cell. The density of water was used for slush, ice and water to avoid a change in cell depth with state as the difference is small (11%) and therefore assumed to be insignificant (Lüthje and others, 2006; Benedek, 2014; Buzzard and others, 2018). A second module deals with snow on the surface when present and incorporates the snow physics of Essery (2015) (see the Snow cover section and Fig. 2) to avoid computationally expensive resizing at each timestep as with Buzzard and others (2018). If the domain depth varies due to meltwater input, a temporary lake insert comprised cells of
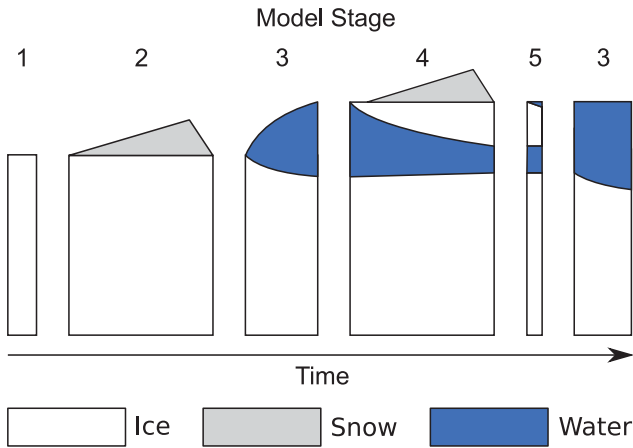
Model Stage

Fig. 1. Schematic diagram of model stages with explanations in Table 1. Width of each stage schematically represents expected residence time. Segment shapes represent schematic evolution of phase throughout stage. The initial section of stage 4 is snow free to show that lid can function with or without snow cover. Height of each column indicates the overall depth of the model domain.

standard size is used within the main cell column (Fig. 2). A bucket filling method is used for each new cell to keep cell sizes uniform, so a new cell is only added when additional meltwater inflow exceeds 10 cm (as default). If the meltwater inflow input ceases, the lake insert is combined with the main column in a one-off operation to reduce complexity in subsequent stages.

Surface energy balance

Surface energy flux in $W\,m^{-2}$ is calculated after Buzzard and others ([2018]) who follow Ebert and Curry ([1993]), as

$$F_{\text{total}} = \varepsilon F_{LW_{\text{in}}} + (1 - \alpha)F_{SW} - \varepsilon\sigma T^4 + F_{\text{sens}} + F_{\text{lat}}, \qquad (1)$$

where ε is the surface emissivity, $F_{LW_{\text{in}}}$ is incoming longwave radiation ($W\,m^{-2}$), α is albedo, F_{SW} is incoming shortwave radiation ($W\,m^{-2}$, separated into water-penetrating and surface radiation when a lake is present using eqn ([12])), σ is the Stefan–Boltzmann constant ($W\,m^{-2}\,K^{-4}$), T is temperature (K), F_{sen} is sensible heat flux ($W\,m^{-2}$) and F_{lat} is latent heat flux ($W\,m^{-2}$). Sensible heat flux is calculated as

$$F_{\text{sens}} = \rho_a C_p^{\text{air}} C_T v (T_a - T_s), \qquad (2)$$

where ρ_a is the density of dry air ($1.275\,\text{kg}\,m^{-3}$), C_p^{air} is the specific heat capacity of dry air ($J\,kg^{-1}\,K^{-1}$), C_T is a function of atmospheric stability described in Ebert and Curry ([1993]) (eqns ([4]) and ([5])), v is the wind speed ($m\,s^{-1}$) and T_a and T_s are air and surface temperature respectively. Latent heat flux is calculated as

$$F_{\text{lat}} = \rho_a L_f C_T v (q_a - q_s), \qquad (3)$$

where L_f is the latent heat of fusion of ice ($J\,kg^{-1}$), and q_a and q_s are the air and surface specific humidities.

C_T is calculated as

$$\begin{cases} C_T = C_{T_s}\left(1 - \dfrac{2b'Ri}{1+c|Ri|^{1/2}}\right) & \text{if } Ri < 0 \\ C_T = C_{T_s}(1 + b'Ri)^{-2} & \text{if } Ri \geq 0, \end{cases} \qquad (4)$$

where $C_{T_s} = 1.3 \times 10^{-3}$, $b' = 20$ and $c = 50.986$ are constants and

Table 1. Description of model stages

Stage	Description
1	Bare ice, no surface snow cover.
2	Snow layer present on top of ice.
3	Lake present above ice.
4	Ice lid overlying lake with/without snow present above.
5	Lid break-up after snowmelt.

Ri is the bulk Richardson number,

$$Ri = \frac{g(T_a - T_s)\Delta z}{T_a v_a^2}, \qquad (5)$$

where Δz is equal to 10 m following Ebert and Curry ([1993]).

Humidity is provided as relative (%) by PROMICE weather stations and converted to specific humidity by first obtaining the saturation vapour pressure, $e_s(T)$ at temperature T (°C), following Tetens ([1930]) as

$$e_s(T) = 0.611 \times 10^{7.5T/(T+237.3)}. \qquad (6)$$

Vapour pressure is obtained using the definition of relative humidity (RH) as

$$e = RH e_s. \qquad (7)$$

The mixing ratio of water vapour, w, is calculated after American Meteorological Society ([2012]) as

$$w = \frac{e R_d}{R_v(p - e)}, \qquad (8)$$

where p is the pressure (Pa), R_d is the specific gas constant for dry air ($J\,kg^{-1}\,K^{-1}$) and R_v is the specific gas constant for water vapour ($J\,kg^{-1}\,K^{-1}$). Lastly, the specific humidity, q, can be obtained after American Meteorological Society ([2012]) using

$$q = \frac{w}{w + 1}. \qquad (9)$$

Lake albedo, α, was calculated following Lüthje and others ([2006]) based on a two-stream approximation from Taylor and Feltham ([2004]) and adapted for the generally lower albedo for glacier ice than sea ice as

$$\alpha = \frac{9702 + 1000e^{3.6z_l}}{-539 + 20000e^{3.6z_l}}, \qquad (10)$$

where z_l is the depth of the lake.

Shortwave propagation

The Beer–Lambert law was used to calculate the transfer of short-wave radiation through water and ice as

$$F_i = F_b e^{-\tau z_i} - F_b e^{-\tau z_{i+1}}, \qquad (11)$$

where F_i is the flux at cell i ($W\,m^{-2}$), τ is the shortwave extinction coefficient (m^{-1}) and z_i is the depth of cell i. F_b, the shortwave radiation entering the water column, is calculated from total incoming shortwave radiation as

$$F_b = I_0(1 - \alpha)F_{sw}, \qquad (12)$$

Table 2. Progression through model stages with brief descriptions of processes occurring at each stage

---

(start)

Import AWS, precipitation, and meltwater input data based on user-specified run time and time step. Initialise arrays, set

state trackers so that correct pathways are taken depending on snow cover, lake insert usage etc., model stage set as 1

Main loop

  If model stage = 1

    Calculate surface energy flux **|** *Phase tracking* **|** *Heat diffusion*

    If sufficient snow has fallen to commence snow layer, move to stage 2

    If top cell is entirely water, move to stage 3

  If model stage = 2

    Incorporate incoming precipitation **|** *Calculate snow melt if required based on phase tracking from previous time step*

    | *Update snow layer density, heat capacity, conductivity and albedo* **|** *Calculate surface energy flux* **|** *Phase tracking*

    | *Heat diffusion*

    If snow has melted, move to stage 3

  If model stage = 3

    Incorporate incoming hydrograph into lake insert **|** *Calculate surface energy flux and shortwave propagation* **|** *Phase*

    tracking **|** *Lake indexing* **|** *Temperature profile* **|** *Turbulence* **|** *Heat diffusion*

    If surface cell has become ice and sufficient snow has fallen to commence snow layer, move to stage 4

  If model stage = 4

    Incorporate incoming precipitation **|** *Calculate snow melt if required based on phase tracking from previous time step*

    | *Update snow-layer density, heat capacity, conductivity and albedo* **|** *Calculate surface energy flux* **|** *Phase tracking*

    | *Lake indexing* **|** *Temperature profile* **|** *Turbulence* **|** *Heat diffusion*

    If lake has frozen, move to stage 2

    If lid is unstable trigger break-up and move to stage 3

    If snow has melted, move to stage 5

  If model stage = 5

    Calculate surface energy flux **|** *Phase tracking* **|** *Lake indexing (two lakes)* **|** *Temperature profiles* **|** *Turbulence* **|** *Heat*

    diffusion

    If lid is unstable trigger break-up and move to stage 3

Plot figures

Trackers monitor events such as initialisation of snow layer to ensure repetition does not occur. Italicised text indicates setup and sub-functions, normal text indicates conditional statements.

where I_0 is the proportion of shortwave radiation absorbed at the lake surface. The net radiation for the surface cell is then reduced to $(1 - I_0)(1 - \alpha)F_{sw}$.

Lake convection and indexing

The lake is modelled as turbulently convecting at ≥ 0.1 m, following Buzzard and others (2018), using the four thirds rule,

$$F_c(T^*) = \text{sign}(\bar{T} - T^*)(\rho C)_l J |\bar{T} - T^*|^{4/3}, \quad (13)$$

where $F_c(T^*)$ is the energy flux at the lake boundary of temperature T^*, $\bar{T}$ is the average lake temperature, $(\rho C)_l$ is the volumetric specific heat capacity of water and J is the turbulent heat flux

factor $(1.907 \times 10^{-5} \text{ ms}^1 \text{ K}^{-1/3})$. Turbulent heat flux is applied to the first slush or ice cell immediately surrounding the lake.

To correctly apply turbulent mixing, correctly indexing slush, ice and water cells was necessary. This was implemented by progressing upwards from the base of the domain and recording the first and last instances of water between ice sections. This prevented two lakes being separated due to any transient appearance of one slush cell in the middle of the lake and encourages slush and ice encroachment from the upper and lower bounds of the lake.

Lake water is stratified based on temperature following the approach of Saloranta and Andersen (2007) by using the UNESCO International Equation of State of Seawater (Loucks and van Beek, 2005). This equation is applicable here as it deals with both saline content and temperature. Once lake input is
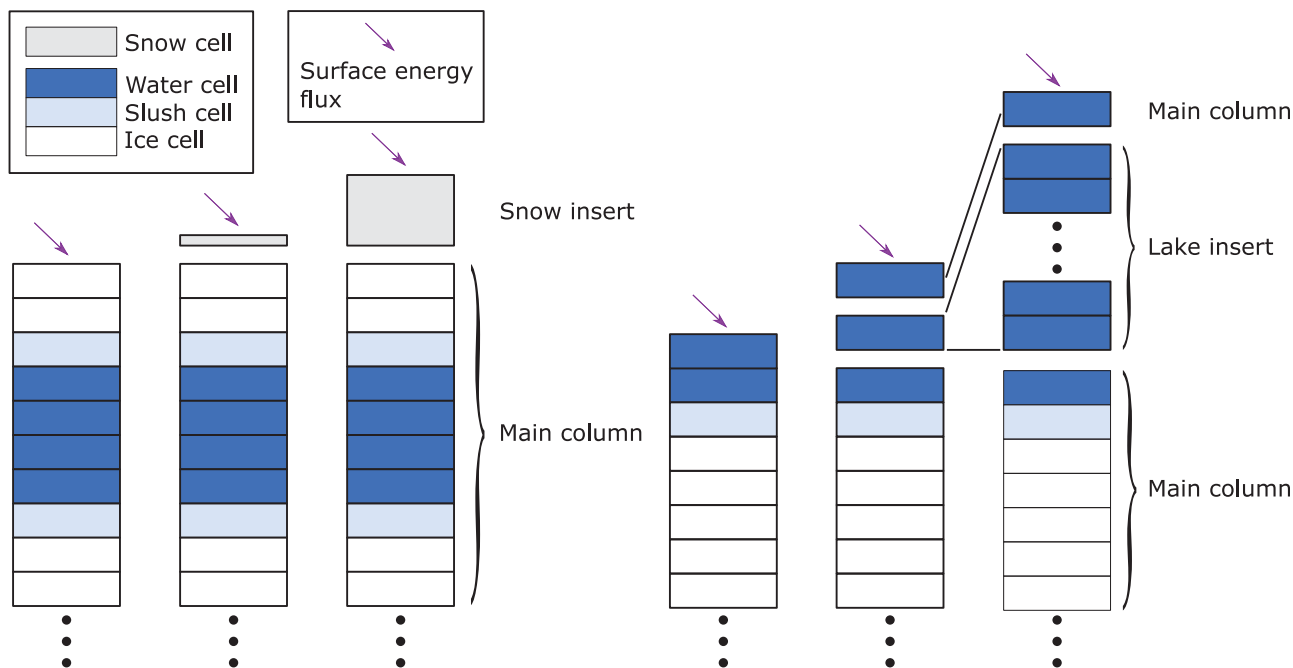
Fig. 2. Construction of separate snow module (left) and the lake insert contained within the main module (right) during meltwater inflow. The lake insert size is increased discretely whereas the snow module size is increased continuously. The lake insert is combined with the main grid after meltwater inflow is complete. The grid size for snow/ice/slush cells remains constant in the upper section of the model but can increase in deeper cells (not shown in this figure).

complete in stage 3 the entire lake insert is combined with the main model domain in a one-off resizing to simplify model code in other stages.

Snow cover

The snow layer is adapted to be coupled to ice, rather than soil as developed by Essery (2015). Further details, including changing snow conductivity, compaction of snow over time, water content calculation and the initialisation of snow conductivity, can be found within Essery (2015). Realistic values for snow density $(200-500\,\mathrm{kg\,m^{-3}})$ are used for the conduction subfunction. Calculations for snow are completed at the beginning of each time step, to allow snow properties to be used subsequently in the conduction subfunction. When the snow layer becomes liquid, the snow layer is eliminated. Following results of sensitivity tests that found the influence of this water to be minor in comparison with meltwater flow into the lake, this water is not introduced into the lake. If refreezing occurs after partial melting of the snow layer, the density and thermal conductivity are updated to account for the proportion of the snow layer that is then solid ice based on the relative proportion of snow, ice and water.

Enthalpy and heat diffusion

By default, the model is initialised as an ice column with temperature linearly interpolated between a surface and basal temperature specified by the user. Temperature is calculated from the cell's enthalpy as below, or in reverse if necessary as

where T_i is the temperature at each grid cell (K), E_i is the enthalpy at each grid cell $(\mathrm{J\,m^{-2}})$, ρ_water is the density of water $(\mathrm{kg\,m^{-3}})$, C_ice is the specific heat capacity of ice $(\mathrm{J(kg\,K)^{-1}})$, C_water is the specific heat capacity of water $(\mathrm{J(kg\,K)^{-1}})$ and $\mathrm{d}z$ is the thickness of the cell. E_{ice_i} and E_{water_i} are the enthalpy thresholds for ice and water respectively $(\mathrm{J\,m^{-2}})$. The model space uses unit metre squares in the x and y direction.

The proportion of each cell that is water, λ_i, is calculated as

$$\begin{cases} \lambda_i = 0 & \text{if } E_i \leq E_{\mathrm{ice}_i} \\ \lambda_i = \frac{E_i - \rho_\mathrm{water} C_\mathrm{ice}\,\mathrm{d}z T_\mathrm{melt} L_f}{\rho_\mathrm{water}\,\mathrm{d}z} & \text{if } E_{\mathrm{ice}_i} < E_i < E_{\mathrm{water}_i} \\ \lambda_i = 1 & \text{if } E_i \geq E_{\mathrm{water}_i}. \end{cases} \quad (15)$$

Heat diffusion is calculated using a backward-time, centred-space approach to enable much longer time steps (tested up to 2 h) whilst maintaining numerical stability when compared to the use of forward-time, centred-space after Lüthje and others (2006) and Alexiades and Solomon (1993). The enthalpy change is calculated from temperature difference at each step, which remains valid unless a cell changes from ice to water or vice versa in one time step (an eventuality which depends on the time step and grid cell thickness and unlikely to occur whilst the model remains stable due to the high latent heat of melting/freezing). The one-dimensional heat diffusion equation,

$$\frac{\partial T}{\partial t} = K \frac{\partial^2 T}{\partial z^2}, \quad (16)$$

$$\begin{cases} T_i = \frac{E_i}{\rho_\mathrm{water} C_\mathrm{ice}\,\mathrm{d}z} & \text{if } E_i \leq E_{\mathrm{ice}_i} \\ T_i = T_\mathrm{melt} & \text{if } E_{\mathrm{ice}_i} < E_i < E_{\mathrm{water}_i} \\ T_i = \frac{E_i}{\rho_\mathrm{water} C_\mathrm{ice}\,\mathrm{d}z} - \frac{1}{C_\mathrm{water}}(C_\mathrm{ice} T_\mathrm{melt} + L_f - C_\mathrm{water} T_\mathrm{melt}) & \text{if } E_i \geq E_{\mathrm{water}_i}, \end{cases} \quad (14)$$

Table 3. Parameters, parameter values and outputs used in sensitivity testing

Parameters	Initial	Lower value	Upper value	Outputs
I_0	0.6	0.4	0.8	Maximum lid thickness (Lid max)
Meltwater inflow multiplier (M_{mult})	1	0	2	Lake depth before lid formation (Lake max)
Albedo multiplier (α_{mult})	1	0.8	1.05	Lake formation day (Lake form)
Initial basal temperature (T_{basal})	-5	-15	-1	Lid formation day (Lid form)
Initial surface temperature ($T_{surface}$)	-4	-10	-1	Lid breakup day (Lid break)
Initial snow density (ρ_{snow})	180	50	250	Maximum average lake temperature (Lake T)
Meltwater inflow temperature (M_T)	0.5	0.2	1.2	

Temperature units are °C, depth and thickness in m and density in $kg\,m^{-3}$.

(here excluding surface energy flux which is incorporated earlier in each timestep) is discretised to allow for non-uniform layer spacing as a result of meltwater input, snowfall and larger deep cells as

$$\frac{T_i^{n+1} - T_i^n}{\Delta t} = K_{i+1/2}^{n+1} \frac{T_{i+1}^{n+1} - T_i^n}{(\Delta z_{i+1/2}^{n+1})^2} - K_{i-1/2}^{n+1} \frac{T_i^{n+1} - T_{i-1}^n}{(\Delta z_{i-1/2}^{n+1})^2}, \quad (17)$$

where n is the time step, i is the cell index, Δx is the distance between the midpoints of two adjacent cells (m) and Δt is the time step. The thermal diffusivity of each cell is calculated as

$$K_i^n = \lambda_i^n K_{water} + (1 - \lambda_i^n)K_{ice}, \quad (18)$$

and the intermediate values between cells are obtained as depth weighted averages. For convenience, eqn (17) is simplified with the use of the S_i^{n+1} term,

$$S_i^{n+1} = K_i^{n+1} \frac{\Delta t}{(\Delta z_i^{n+1})^2}, \quad (19)$$

to give

$$T_i^n = -S_{i+1/2}^{n+1} T_{i+1}^{n+1} + (1 + S_{i+1/2}^{n+1} + S_{i-1/2}^{n+1})T_i^{n+1} - S_{i-1/2}^{n+1} T_{i-1}^{n+1}. \quad (20)$$

A zero-flux boundary condition was specified for the base of the domain with the ice temperature of the bottom cell initially set at $-5°C$. The default size of the upper cells is 0.1 m, enlarged to 1 m for the lowermost 30 cells to allow a large spatial domain without significantly increasing run-time. Equation (20) can then be entered into a system of simultaneous equations using a tridiagonal matrix generalised to a given number of model layers and solved as a matrix equation at each time step. The temperature of the surface cell is updated at each time step according to eqn (1) prior to heat diffusion.

Model testing

Sensitivity testing

Testing was conducted to determine the sensitivity of important GlacierLake outputs to parameter uncertainty. Normalised sensitivity coefficients for seven input parameters and six important output measures (Table 3) were calculated following Loucks and van Beek (2005) as

$$\frac{|Q(P_0 + \Delta P) - Q(P_0 - \Delta P)|}{2\Delta P} \times \frac{P_0}{Q(P_0)}, \quad (21)$$

where $Q(P_0 \pm \Delta P)$ is the output value Q when forced with a
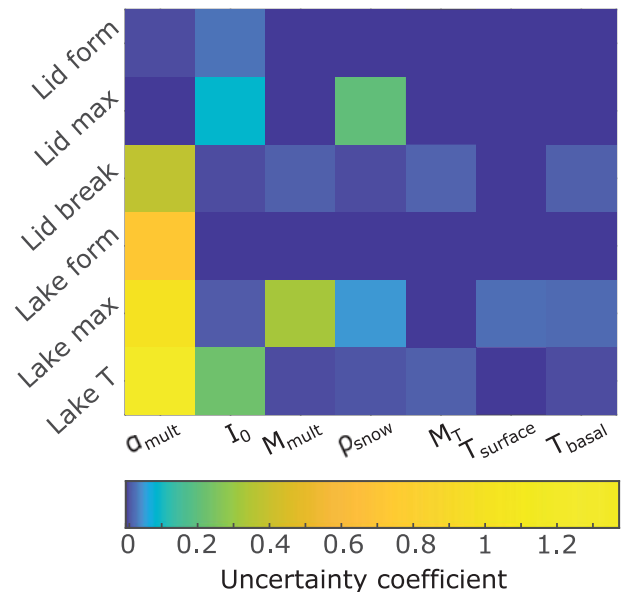

Fig. 3. Inter-comparison of sensitivity coefficients. Ordered by greatest sum uncertainty in columns and then rows. Abbreviations shown in Table 3. Note exponential scale for colour bar.

parameter of value $P_0 \pm \Delta P$, P_0 is the initial parameter value and ΔP is variation away from P_0.

Figure 3 shows sensitivity coefficients. Most uncertainty is confined to albedo and the I_0 term (proportion of shortwave radiation absorbed at the lake surface) with the model output being fairly insensitive (sensitivity coefficient ≤0.2 excluding lake depth sensitivity to meltwater input) to other parameters. Many parameters are hard to obtain precisely and are subject to temporal and spatial variability, so this low sensitivity to parameter uncertainty promotes confidence in GlacierLake's results. The I_0 term merits further consideration and is covered in the discussion.

Tuning

The only published in-situ measurements of lake bottom ablation and lake depth come from Tedesco and others (2012); data which were also used by Banwell and others (2012a). The record from Lake Ponting (69.589 N, -49.783 E, 962 m, data from 15th–19th June 2011) was compared to a GlacierLake run from 24th September 2009–1st August 2010, which was driven with GC-Net AWS data as processed by Banwell and others (2012b), with incoming long wave radiation calculated at each time step within GlacierLake using equations from Banwell and others (2012b). For precipitation input, RACMO2.3p2 was used (Noël and others, 2018). The change in the I_0 value resulted in a large variation in the model output. An I_0 value of 0.8, slightly greater than the value of 0.6 used by Lüthje and others (2006), Tedesco and others (2012), Benedek (2014) and Buzzard and
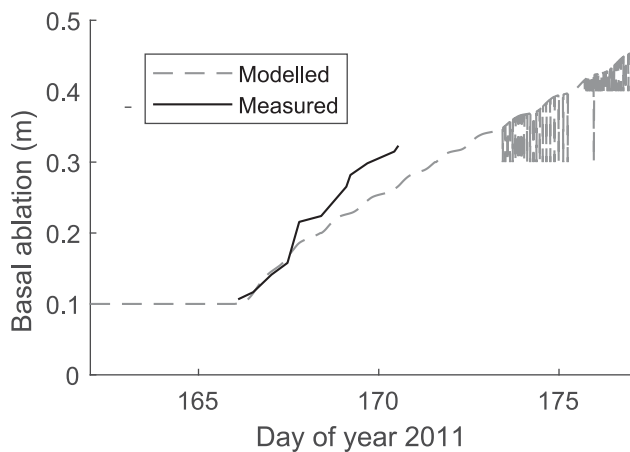
Fig. 4. Comparison of modelled lake bottom ablation to measured lake bottom ablation data from Tedesco and others (2012). Dashed light grey is modelled basal ice ablation excluding lake formation, black is measured lake bottom ablation. Jumps in modelled ablation around day 175 result from threshold behaviour with cell enthalpy near the slush-water boundary.

others (2018) produced the output seen in Fig. 4. Values set as default following tuning can be found within the main function of the supplied code. GlacierLake is not intended to predict the evolution of specific, individual lakes with absolute accuracy, but this test shows that it is well suited for modelling broad trends and for understanding the behaviour of supraglacial lakes in Greenland. Large-scale comparison to remotely sensed lid thickness is beyond the scope of this study.

Air temperature and precipitation variation

Precipitation and temperature vary across the spatial domain of lake occurrence in Greenland (Bromwich and others, 2001; Gledhill and Williamson, 2017) and exert strong controls over ice lid formation within GlacierLake. While arbitrary, the following temperature and precipitation ranges were chosen to observe the behaviour of GlacierLake within, and slightly beyond, conditions where supraglacial lakes may reasonably be expected to form across the GrIS. Testing the relative importance of precipitation and temperature on lid formation enables a range of expected lid thicknesses at the beginning of the melt season to be obtained, as well as to find if any threshold behaviour is apparent. Weather data from PROMICE UPE U, with 2 m total of meltwater input (over 5 days using Lake Ponting data from Tedesco and others, 2012) was used to form a lake with conditions varied upon lid formation to simulate the effect of precipitation and temperature differences on lid formation from a common starting point. Precipitation was multiplied by a factor ranging from 0 to 3 resulting in start of melt season snow depths between 0 and 3.45 m. Temperature from the day of lid formation to the end of the model run was added to or subtracted to with a range from +10 to −20°C. Average temperature over this period with default settings is −12.4°C giving a range from −2.4 to −32.4°C. The maximum lid thickness before lid breakup (or at 298 days of lid coverage if no lid breakup occurs) was recorded for a range of 25 inputs for precipitation and temperature giving 625 values in total.

Figure 5 shows that a change in snow cover between 0 and 3.9 m over winter while air temperature is constant results in a greater range of ice lid thickness than a change in over-winter temperature between +10 and −20°C (0.8–2.5 m against 1.4–2.3 m). Lid thickness varies smoothly with a parameter change with no threshold behaviour observed. Figure 5 also shows that even under the most extreme conditions tested (no
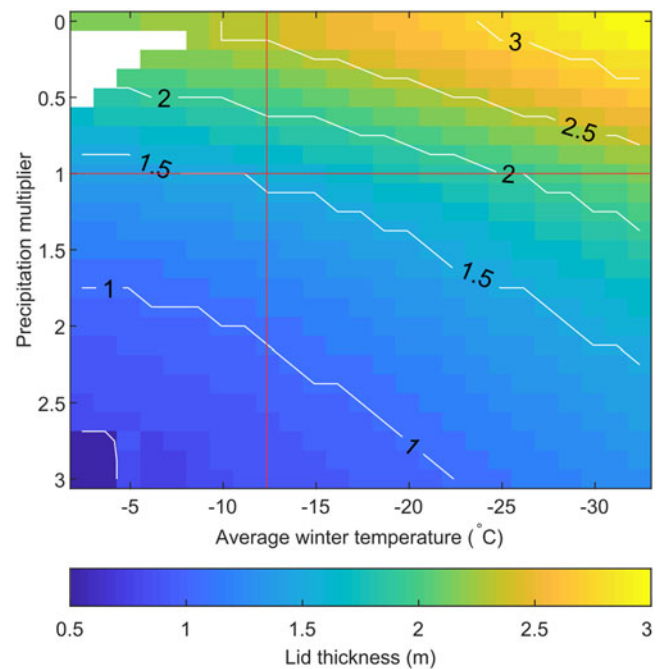

Fig. 5. Change in the maximum lid thickness with temperature and precipitation variation. Red vertical and horizontal lines indicate default UPE U conditions. White is where lid formation malfunctioned within GlacierLake. White contours show 0.5 m maximum thickness intervals.

snow cover and average winter temperatures of −32.4°C) lid thickness does not exceed 3.3 m. Koenig and others (2015) find an average ice lid thickness of 1.4 m, with 0.65 m of snow cover present using observations obtained through Operation IceBridge. GlacierLake predicts lid thickness ranging from 1.7–2.7 m depending on temperature when snow cover at the start of the melt season reaches 0.65 m Koenig and others (2015). This translates to thinner lids (1.5–2.5 m) during April and May when IceBridge flights are performed but suggests GlacierLake may slightly over predict lid thickness.

Advection and basal freeze-up

Although GlacierLake does not have inbuilt allowance for advection, its effect was simulated by resetting ice temperature to its initial value on the day of lid formation, effectively removing the impact of warming earlier in the model run (Fig. 6). As surface energy flux is effectively isolated from the base upon lid formation this represents the earliest time in the model run where near-surface temperatures are not atmospherically controlled (e.g. cold wave in Fig. 6, left). A lower temperature limit of −15°C was chosen as limited near-surface ice temperature profiles of land terminating sectors of the GrIS show this to be at the lower end of expected values (Meierbachtol and others, 2013). Figure 7 shows that including advection increases basal freeze-up by at most 0.1 m compared to runs with no simulated advection. Total basal freeze-up with an initial ice temperature of −15°C is limited to 0.5 or 0.6 m with simulated advection. Altering the initial and advecting ice temperature made no difference to the magnitude of lid freezing (constant at 1.6 m throughout the test).

Temperature change at depth

The assumption that the warming influence of supraglacial lakes on underlying ice is not significant (Poinar and others, 2017) has not been tested in the literature. We examine this by extending the
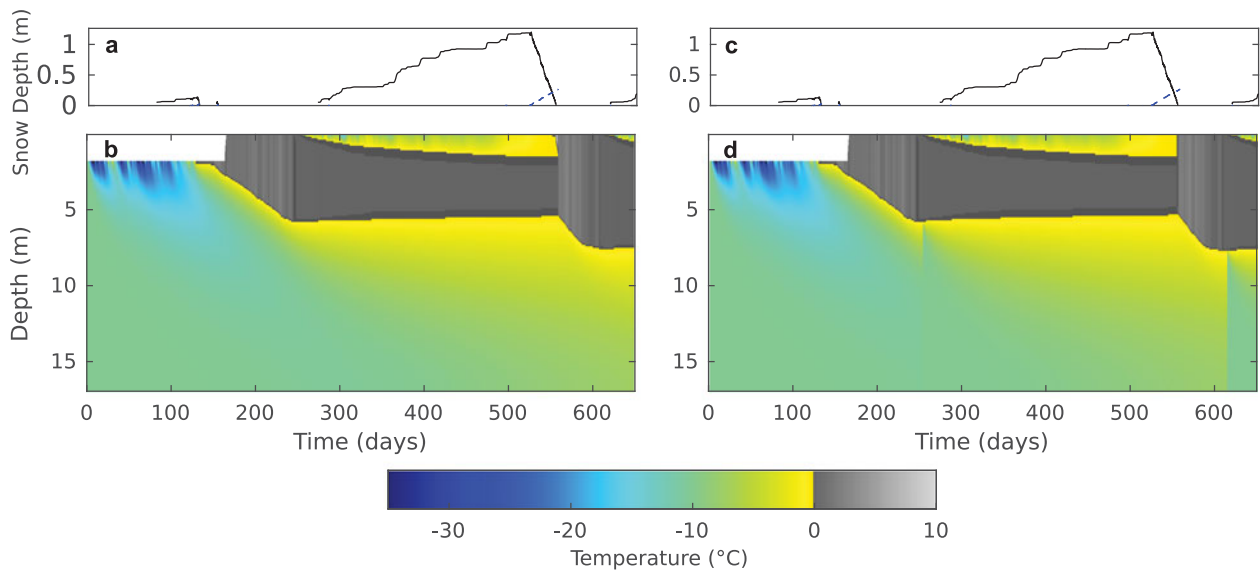
Fig. 6. Simulated advection. Panels a and b: no alteration to ice temperature initially set at −10°C. Panels c and d: a constant temperature of −10°C was set initially, and repeated upon lid formation. Basal freeze-up was 0.4 and 0.5 m respectively. White space in panels b and d is free space before meltwater inflow input. Black line in panels a and c is snow depth, dashed blue line is water depth in snow layer.
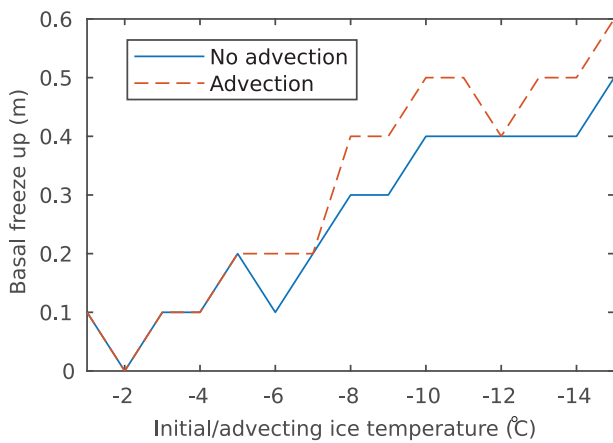

Fig. 7. Total basal freeze-up whilst lid is present (stages 4–5) with and without simulated advection. Whilst the trend is upwards, small decreases in basal freeze-up are observed with and without advection included. This is a result of threshold behaviour between slush, water and ice within cells where the temperature is at, or within 0.05°C of 0°C. For example a colder initial ice temperature may result in an increase of three slush cells above the ice-slush boundary but a decrease of one ice cell. Refer to Fig. 6 for test setup.

1 m deep cells at the bottom of the model to a total of 50 m (Fig. 8) making a 60 m domain in total. The initial temperature profile is set uniformly to −10°C with weather data from PROMICE station UPE-U (Fausto and van As, 2019). Figure 8 shows the lake exerts a strong influence (up to 8°C) to around 10 m below the lake, however the warming effect beyond 15 m below the lake is limited at less than 1°C.

GlacierLake behaviour at UPE-U AWS

To test steady-state behaviour, and the general behaviour of GlacierLake, it was run with PROMICE UPE-U data for 1000 days from 1st of January, 2010, repeating forcing data year on year. Figure 9 shows that although the thermal impact of a lake on underlying ice is limited beyond 15 m it is sufficient to prompt faster lake formation the following melt season. As annual melt exceeds annual refreezing, no steady state arises.
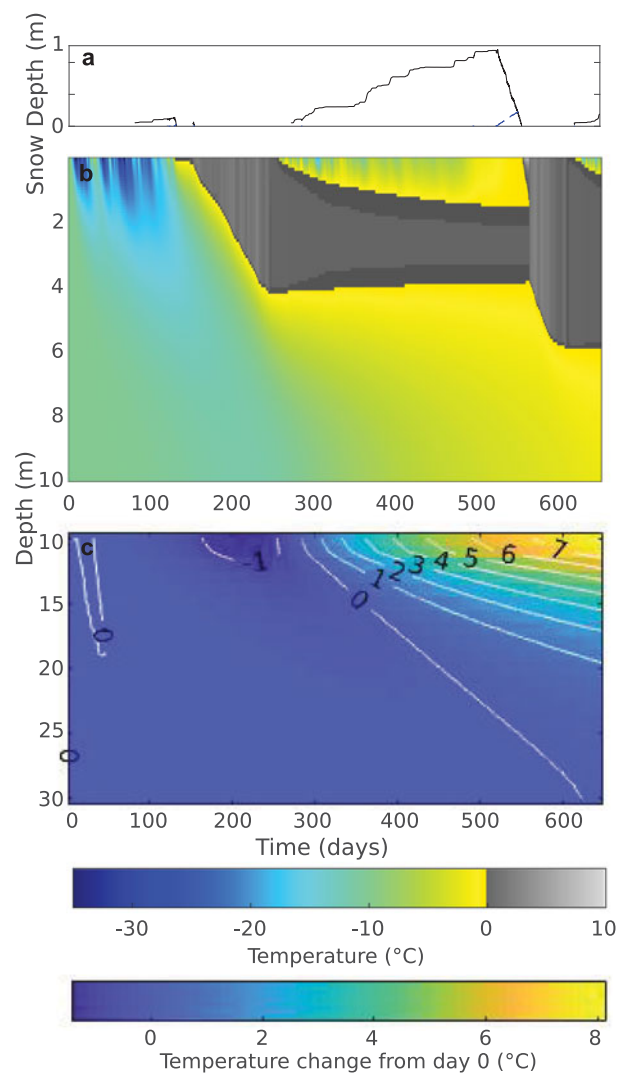
Fig. 8. Ice temperature at depth using AWS data from the PROMICE UPE-U weather station, commencing 1st January 2010. Note the change in depth scale and jump from absolute temperature to temperature change from day 0 between panels b and c. Although the overall model domain extends to 60 m, only the upper 30 m are shown here. Black line in panel a is snow depth, blue dashed line is water depth.
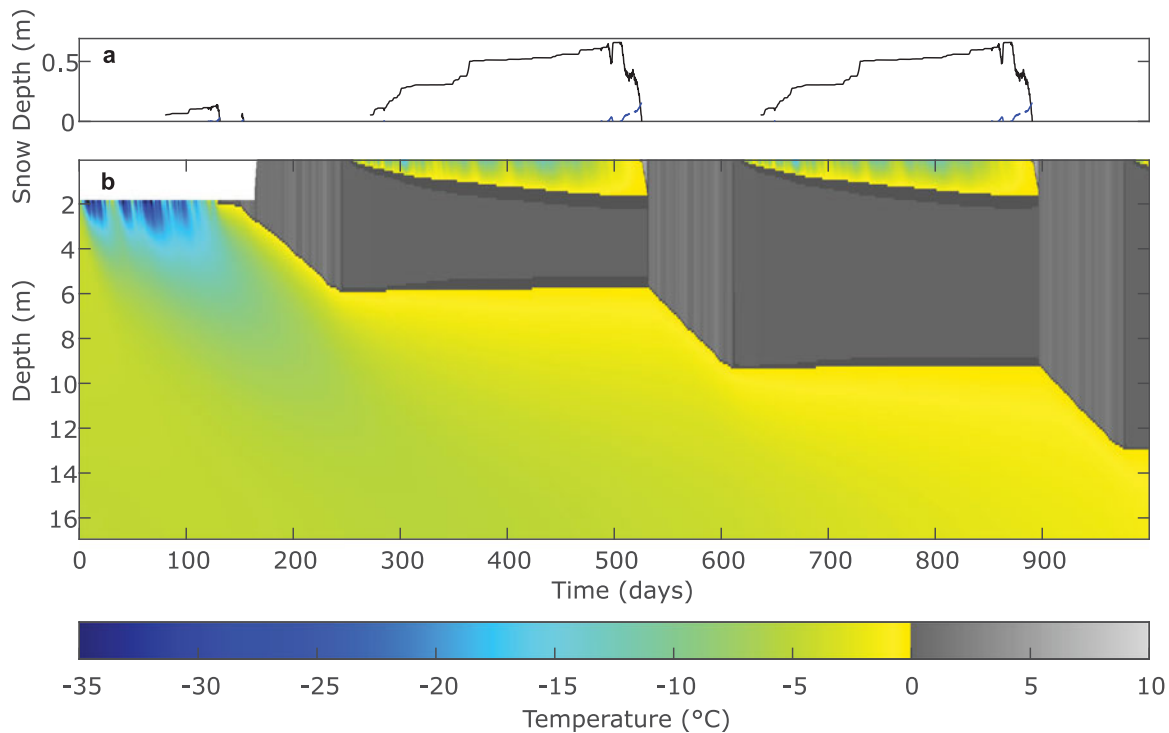
Fig. 9. Example model output including a short duration meltwater inflow input and snow cover, with data from PROMICE UPE-U AWS from 1st January 2010 repeating year-on-year for 1000 days. Panel a shows snow cover where black is snow depth and dashed blue is water depth. Panel b showsa lake temperature profile. White space in panel b is free space before meltwater inflow input.

Discussion

Temperature change at depth and multi-year behaviour

Warming of ice beneath lakes (Fig. 8) may influence lake drainage events on the GrIS as the fracture toughness of ice decreases with warming ice (Liu and Miller, 1979), potentially lowering the stress threshold for fracture propagation beneath lakes (Krawczynski and others, 2009). However, further studies would be required to accurately assess this possibility. Figure 9 shows no steady state arises, consistent with melt rates of metres per year in the ablation zone. This points to lake drainage by fracture or over-topping being important controls in limiting the depth of lakes on the GrIS, as has been previously observed (Tedesco and Fettweis, 2012) and also modelled (Banwell and others, 2012a). When buried, the lake top and bottom act as a 0°C boundaries, for both the underlying ice and the overlying ice lid. The consequence of this on the ice lid is to prevent very cold mid-winter temperatures due to an upward energy flux from latent heat of freezing of the water. This, with colder temperatures at the top of the water profile, contributes to lid freezing outpacing basal freeze-up.

I_0 term

Figures 3 and 4 show that model sensitivity to the value of I_0 is large, suggesting it should tested before model use where possible. The use of the I_0 term has moved away from its initial model implementation in Ebert and Curry (1993) who use I_0 in the Beer–Lambert law when calculating shortwave energy absorption in ice with brine pockets. When a meltwater lake is present Ebert and Curry (1993) instead use the equation

$$F_p = F_{SW}\left[a_p + a_p \alpha_i t_p + t_p(1 - \alpha_i)(1 - I_0)\right], \quad (22)$$

where a_p is the proportion of shortwave absorbed by the pond, α_i is bare ice albedo, t_p is the pond transmissivity as a function

of depth and I_0 is the fraction of shortwave to penetrate the ice. They take an I_0 value that varies with cloud cover, with a maximum value of 0.35 under cloudy skies and a minimum value of 0.18 under clear skies, following Grenfell and Maykut (1977). This reflects the fact that there is more incoming radiation in the infrared range under clear skies, most of which is absorbed in the upper 10 cm of the ice profile (Grenfell and Maykut, 1977).

Lüthje and others (2006) deviate and take I_0 as the proportion of shortwave radiation that propagates below the surface water layer, as does this model. Lüthje and others (2006) use 0.6 as the value of I_0 as Grenfell and Maykut (1977) find the fraction of incident shortwave radiation above 700 nm (i.e. infrared) to be 40% (in disagreement with Kirk, 1988 who suggests a value of 50%). Their value of 0.6 is chosen as infrared radiation is strongly absorbed by the top 0.5 m of the water (Kirk, 1988). The calculation of Lüthje and others (2006) however, excludes reflection from the bare ice surface so may result in an oversupply of shortwave radiation to the upper ice layers beneath the lake. Lüthje and others (2006) do not run sensitivity tests of the I_0 value and it is subsequently used in Tedesco and others (2012), Buzzard and others (2018) and the sea-ice lake model of Scott and Feltham (2010), without further testing.

The I_0 term is important as it determines a proportion of incoming shortwave radiation, $F_{SW}(1 - I_0)$, which will not be factored into the Beer–Lambert law and will therefore not be accessible to the underlying ice. The large sensitivity coefficients arises as a greater I_0 means a greater energy flux for the upper ice cells, as shortwave infiltration is a faster transfer mechanism than turbulent heat transfer and heat diffusion. In effect, the use of the I_0 term here is equivalent to an original I_0 value (as intended by Ebert and Curry, 1993) of 1 (i.e. all shortwave radiation enters the water column), with a certain fraction of light that penetrates to the lake base reflected backwards. In light of these points, the I_0 term in its form used here was adjusted to obtain the closest match with measured basal ablation. Future models could

re-incorporate the I_0 definition of Ebert and Curry (1993) or take note of the terms sensitivity. Discussion of the importance of the I_0 term in low melt/ablation bare ice is covered in Hoffman and others (2014).

Conclusion

This study has presented the first model for the full multi-year evolution of supraglacial lakes in the ablation zone of the GrIS. GlacierLake can replicate field data for ablation and lake formation from Tedesco and others (2012) with lid thickness slightly exceeding observations from Koenig and others (2015) when a snow thickness of 0.65 m is used. GlacierLake shows that the sum of the ice-lid thickness and basal freeze-up is unlikely to exceed 3.9 m with no snow cover, or 2.8 m with 1 m of snow cover at the end of the melt season. This represents an important physically based confirmation of Koenig and others (2015), i.e. that a large number of lakes can be expected to remain (at least partially) unfrozen throughout the winter, with implications for the development of the supraglacial hydrological system in the following melt season due to a pre-existing water stores. The computational efficiency of GlacierLake means it could be incorporated into a holistic model of Greenland supraglacial hydrology without impeding run time, and that it could be easily used in ice sheet-wide studies. GlacierLake could also be easily adapted to valley glacier or ice-cap supraglacial lakes. Sensitivity testing reveals the importance of the I_0 (proportion of shortwave radiation absorbed at the lake surface) term in determining energy transfer to the base of the lake. The results presented here are vital for better understanding the role of lakes for surrounding ice temperatures and in forming surface-bed links through lake hydrofracture. It is hoped that this study will provide an overall better understanding of GrIS surface-melt processes; such processes ultimately drive a significant and accelerating component of global sea-level rise.

References

Alexiades V and Solomon AD (1993) *Mathematical modeling of melting and freezing processes.* Washington: Hemisphere Pub. Corp.

AMAP (2017) Snow, Water, Ice and Permafrost. Summary for Policy-makers | AMAP. Technical report, Arctic Monitoring and Assessment Programme, Oslo, Norway.

American Meteorological Society (2012) Mixing ratio - AMS Glossary.

Arnold NS, Banwell AF and Willis IC (2014) High-resolution modelling of the seasonal evolution of surface water storage on the Greenland Ice Sheet. *Cryosphere* 8(4), 1149–1160. doi: 10.5194/tc-8-1149-2014

Banwell A, Hewitt I, Willis I and Arnold N (2016) Moulin density controls drainage development beneath the Greenland ice sheet. *Journal of Geophysical Research: Earth Surface* 121(12), 2248–2269. doi: 10.1002/2015JF003801

Banwell AF, Arnold NS, Willis IC, Tedesco M and Ahlstrøm AP (2012a) Modeling supraglacial water routing and lake filling on the Greenland Ice Sheet. *Journal of Geophysical Research: Earth Surface* 117(F4), F04012. doi: 10.1029/2012JF002393

Banwell AF and 6 others (2012b) Calibration and evaluation of a high-resolution surface mass-balance model for Paakitsoq, West Greenland. *Journal of Glaciology* 58(212), 1047–1062. doi: 10.3189/2012JoG12J034

Benedek C (2014) Enhanced melting beneath supra-glacial lakes on the Greenland Ice Sheet. (PhD thesis, University of Cambridge).

Box JE and Ski K (2007) Remote sounding of Greenland supraglacial melt lakes: implications for subglacial hydraulics. *Journal of Glaciology* 53 (181), 257–265. doi: 10.3189/172756507782202883

Bromwich DH, Chen QS, Bai LS, Cassano EN and Li Y (2001) Modeled precipitation variability over the Greenland Ice Sheet. *Journal of Geophysical Research: Atmospheres* 106(D24), 33891–33908. doi: 10.1029/2001JD900251

Buzzard S, Feltham D and Flocco D (2018) A mathematical model of Melt Lake Development on an Ice Shelf. *Journal of Advances in Modeling Earth Systems* 10(2), 262–283. doi: 10.1002/2017MS001155

Catania GA and Neumann TA (2010) Persistent englacial drainage features in the Greenland Ice Sheet. *Geophysical Research Letters* 37(2), L02501. doi: 10.1029/2009GL041108

Chu VW (2014) Greenland ice sheet hydrology. *Progress in Physical Geography* 38(1), 19–54. doi: 10.1177/0309133313507075

Das SB and 6 others (2008) Fracture propagation to the base of the Greenland Ice Sheet during supraglacial lake drainage. *Science (New York, N.Y.)* 320 (5877), 778–781. doi: 10.1126/science.1153360

De La Peña S and 8 others (2015) Changes in the firn structure of the western Greenland Ice Sheet caused by recent warming. *The Cryosphere* 9, 1203–1211. doi: 10.5194/tc-9-1203-2015

Doyle SH and 9 others (2013) Ice tectonic deformation during the rapid in situ drainage of a supraglacial lake on the Greenland Ice Sheet. *The Cryosphere* 7(1), 129–140. doi: 10.5194/tc-7-129-2013

Ebert EE and Curry JA (1993) An intermediate one-dimensional thermodynamic sea ice model for investigating ice-atmosphere interactions. *Journal of Geophysical Research* 98(C6), 10085. doi: 10.1029/93JC00656

Echelmeyer K, Clarke TS and Harrison W (1991) Surficial glaciology of Jakobshavns Isbræ, West Greenland: Part I. Surface morphology. *Journal of Glaciology* 37(127), 368–382. doi: 10.3189/S0022143000005803

Essery R (2015) A factorial snowpack model (FSM 1.0). *Geoscientific Model Development* 8(12), 3867–3876. doi: 10.5194/gmd-8-3867-2015

Fausto R and van As D (2019) Programme for monitoring of the Greenland ice sheet (PROMICE): Automatic weather station data. Version: v03 (doi: 10.22008/promice/data/aws).

Fetterer F and Untersteiner N (1998) Observations of melt ponds on Arctic sea ice. *Journal of Geophysical Research: Oceans* 103(C11), 24821–24835. doi: 10.1029/98JC02034

Fitzpatrick AAW and 9 others (2014) A decade (2002–2012) of supraglacial lake volume estimates across Russell Glacier, West Greenland. *The Cryosphere* 8(1), 107–121. doi: 10.5194/tc-8-107-2014

Forster RR and 12 others (2014) Extensive liquid meltwater storage in firn within the Greenland ice sheet. *Nature Geoscience* 7(2), 95–98. doi: 10.1038/ngeo2043

Gledhill LA and Williamson AG (2017) Inland advance of supraglacial lakes in north-west Greenland under recent climatic warming. *Annals of Glaciology* 59(76pt1), 66–82. doi: 10.1017/aog.2017.31

Grenfell TC and Maykut GA (1977) The optical properties of ice and snow in the Arctic Basin. *Journal of Glaciology* 18(80), 445–463. doi: 10.3189/S0022143000021122

Hills BH, Harper JT, Humphrey NF and Meierbachtol TW (2017) Measured horizontal temperature gradients constrain heat transfer mechanisms in Greenland Ice. *Geophysical Research Letters* 44(19), 9778–9785. doi: 10.1002/2017GL074917

Hoffman MJ, Fountain AG and Liston GE (2014) Near-surface internal melting: a substantial mass loss on Antarctic Dry Valley glaciers. *Journal of Glaciology* 60(220), 361–374. doi: 10.3189/2014JoG13J095

Hoffman MJ and 7 others (2018) Widespread moulin formation during supraglacial lake drainages in Greenland. *Geophysical Research Letters* 45 (2), 778–788. doi: 10.1002/2017GL075659

The IMBIE Team (2019) Mass balance of the Greenland Ice Sheet from 1992 to 2018. *Nature.* doi: 10.1038/s41586-019-1855-2

Jacob T, Wahr J, Pfeffer WT and Swenson S (2012) Recent contributions of glaciers and ice caps to sea level rise. *Nature* **482**(7386), 514–518. doi: 10.1038/nature10847

Johansson A, Jansson P and Brown I (2013) Spatial and temporal variations in lakes on the Greenland Ice Sheet. *Journal of Hydrology* **476**, 314–320. doi: 10.1016/J.JHYDROL.2012.10.045

Kirk JTO (1988) Solar heating of water bodies as influenced by their inherent optical properties. *Journal of Geophysical Research* **93**(D9), 10897–10908.

Koenig LS and 11 others (2015) Wintertime storage of water in buried supraglacial lakes across the Greenland Ice Sheet. *The Cryosphere* **9**(4), 1333–1342. doi: 10.5194/tc-9-1333-2015

Koziol C, Arnold N, Pope A and Colgan W (2017) Quantifying supraglacial meltwater pathways in the Paakitsoq region, West Greenland. *Journal of Glaciology* **63**(239), 464–476. doi: 10.1017/jog.2017.5

Koziol CP and Arnold N (2018) Modelling seasonal meltwater forcing of the velocity of land-terminating margins of the Greenland Ice Sheet. *The Cryosphere* **12**(3), 971–991. doi: 10.5194/tc-12-971-2018

Krawczynski MJ, Behn MD, Das SB and Joughin I (2009) Constraints on the lake volume required for hydro-fracture through ice sheets. *Geophysical Research Letters* **36**(10), L10501. doi: 10.1029/2008GL036765

Lampkin DJ and VanderBerg J (2011) A preliminary investigation of the influence of basal and surface topography on supraglacial lake distribution near Jakobshavn Isbrae, western Greenland. *Hydrological Processes* **25**(21), 3347–3355. doi: 10.1002/hyp.8170

Leeson AA and 6 others (2015) Supraglacial lakes on the Greenland ice sheet advance inland under warming climate. *Nature Climate Change* **5**(1), 51–55. doi: 10.1038/nclimate2463

Liang YL and 7 others (2012) A decadal investigation of supraglacial lakes in West Greenland using a fully automatic detection and tracking algorithm. *Remote Sensing of Environment* **123**, 127–138. doi: 10.1016/J.RSE.2012.03.020

Liu HW and Miller KJ (1979) Fracture toughness of fresh-water ice. *Journal of Glaciology* **22**(86), 135–143. doi: 10.3189/S0022143000014118

Loucks D and van Beek E (2005) *UNESCO - Water Resources Systems Planning; Management, 2005*. Technical report, UNESCO.

Lüthje M, Feltham DL, Taylor PD and Worster MG (2006) Modeling the summertime evolution of sea-ice melt ponds. *Journal of Geophysical Research: Oceans* **111**(C2), C02001. doi: 10.1029/2004JC002818

Lüthi MP and 7 others (2015) Heat sources within the Greenland Ice Sheet: dissipation, temperate paleo-firn and cryo-hydrologic warming. *The Cryosphere* **9**, 245–253. doi: 10.5194/tc-9-245-2015

Mayaud JR, Banwell AF, Arnold NS and Willis IC (2014) Modeling the response of subglacial drainage at Paakitsoq, west Greenland, to 21st century climate change. *Journal of Geophysical Research: Earth Surface* **119**(12), 2619–2634. doi: 10.1002/2014JF003271

Maykut GA and Untersteiner N (1971) Some results from a time-dependent thermodynamic model of sea ice. *Journal of Geophysical Research* **76**(6), 1550–1575. doi: 10.1029/JC076i006p01550

McMillan M, Nienow P, Shepherd A, Benham T and Sole A (2007) Seasonal evolution of supra-glacial lakes on the Greenland Ice Sheet. *Earth and Planetary Science Letters* **262**(3–4), 484–492. doi: 10.1016/J.EPSL.2007.08.002

Meierbachtol T, Harper J and Humphrey N (2013) Basal drainage system response to increasing surface melt on the Greenland ice sheet. *Science (New York, N.Y.)* **341**(6147), 777–779. doi: 10.1126/science.1235905

Mikkelsen AB and 9 others (2016) Extraordinary runoff from the Greenland ice sheet in 2012 amplified by hypsometry and depleted firn retention. *The Cryosphere* **10**(3), 1147–1159. doi: 10.5194/tc-10-1147-2016

Miles KE, Willis IC, Benedek CL, Williamson AG and Tedesco M (2017) Toward Monitoring Surface and Subsurface Lakes on the Greenland Ice Sheet Using Sentinel-1 SAR and Landsat-8 OLI Imagery. *Frontiers in Earth Science* **5**(58), 1–17. doi: 10.3389/feart.2017.00058

Morassutti MP and Ledrew EF (1996) Albedo and depth of melt ponds on sea-ice. *International Journal of Climatology* **16**(8), 17–838.

Nienow PW, Sole AJ, Slater DA and Cowton TR (2017) Recent advances in our understanding of the role of meltwater in the Greenland Ice Sheet System. *Current Climate Change Reports* **3**(4), 330–344. doi: 10.1007/s40641-017-0083-9

Noël B and 9 others (2017) A tipping point in refreezing accelerates mass loss of Greenland's glaciers and ice caps. *Nature Communications* (14730), 1–8. doi: 10.1038/ncomms14730

Noël B and 11 others (2018) Modelling the climate and surface mass balance of polar ice sheets using RACMO2 – Part 1: Greenland (1958–2016). *The Cryosphere* **12**, 811–831. doi: 10.5194/tc-12-811-2018

Phillips T, Rajaram H and Steffen K (2010) Cryo-hydrologic warming: A potential mechanism for rapid thermal response of ice sheets. *Geophysical Research Letters* **37**(20), L20503. doi: 10.1029/2010GL044397

Phillips T, Rajaram H, Colgan W, Steffen K and Abdalati W (2013) Evaluation of cryo-hydrologic warming as an explanation for increased ice velocities in the wet snow zone, Sermeq Avannarleq, West Greenland. *Journal of Geophysical Research: Earth Surface* **118**(3), 1241–1256. doi: 10.1002/jgrf.20079

Poinar K, Joughin I, Lenaerts JTM and Van Den Broeke MR (2017) Englacial latent-heat transfer has limited influence on seaward ice flux in western Greenland. *Journal of Glaciology* **63**(237), 1–16. doi: 10.1017/jog.2016.103

Rennermalm AK and 11 others (2013) Understanding Greenland ice sheet hydrology using an integrated multi-scale approach. *Environmental Research Letters* **8**(1), 0150171–14. doi: 10.1088/1748-9326/8/1/015017

Rignot E, Velicogna I, van den Broeke MR, Monaghan A and Lenaerts JTM (2011) Acceleration of the contribution of the Greenland and Antarctic ice sheets to sea level rise. *Geophysical Research Letters* **38**(5), L05503. doi: 10.1029/2011GL046583

Russell AJ (1993) Supraglacial lake drainage near Sendre Strømjford, Greenland. *Journal of Glaciology* **39**(132), 431–433. doi: 10.3189/S0022143000016105

Saloranta TM and Andersen T (2007) MyLake—A multi-year lake simulation model code suitable for uncertainty and sensitivity analysis simulations. *Ecological Modelling* **207**(1), 45–60. doi: 10.1016/J.ECOLMODEL.2007.03.018

Scott F and Feltham DL (2010) A model of the three-dimensional evolution of Arctic melt ponds on first-year and multiyear sea ice. *Journal of Geophysical Research* **115**(C12), C12064. doi: 10.1029/2010JC006156

Selmes N, Murray T and James TD (2013) Characterizing supraglacial lake drainage and freezing on the Greenland Ice Sheet. *The Cryosphere Discussions* **7**(1), 475–505. doi: 10.5194/tcd-7-475-2013

Skyllingstad ED, Paulson CA and Perovich DK (2009) Simulation of melt pond evolution on level ice. *Journal of Geophysics Research* **114**, C12019. doi: 10.1029/2009JC005363

Steger CR and 11 others (2017) Firn meltwater retention on the Greenland Ice Sheet: a model comparison. *Frontiers in Earth Science* **5**(3), 1–16. doi: 10.3389/feart.2017.00003

Taylor PD and Feltham DL (2004) A model of melt pond evolution on sea ice. *Journal of Geophysical Research* **109**, C12007. doi: 10.1029/2004JC002361

Tedesco M and 7 others (2012) Measurement and modeling of ablation of the bottom of supraglacial lakes in western Greenland. *Geophysical Research Letters* **39**, L02502. doi: 10.1029/2011GL049882

Tedesco M and 5 others (2013) Ice dynamic response to two modes of surface lake drainage on the Greenland ice sheet. *Environmental Research Letters* **8** 0340071–9. doi: 10.1088/1748-9326/8/3/034007

Tedesco M and Fettweis X (2012) 21st century projections of surface mass balance changes for major drainage systems of the Greenland ice sheet. *Environmental Research Letters* **7**, 045405. doi: 10.1088/1748-9326/7/4/045405

Tetens O (1930) Uber einige meteorologische Begriffe. *Zeitschrift fur Geophysik* **6**, 297–309.

van As D, Fausto R and PROMICE project team, t (2010) Geological Survey of Denmark and Greenland Bulletin 23 (2011), 73–76. Technical report, Geological Survey of Denmark and Greenland.

van den Broeke MR and 7 others (2016) On the recent contribution of the Greenland ice sheet to sea level change. *The Cryosphere* **10**(5), 1933–1946. doi: 10.5194/tc-10-1933-2016

Vernon CL and 6 others (2013) Surface mass balance model intercomparison for the Greenland ice sheet. *The Cryosphere* **7**, 599–614. doi: 10.5194/tc-7-599-2013

Williamson AG, Banwell AF, Willis IC and Arnold NS (2018a) Dual-satellite (Sentinel-2 and Landsat 8) remote sensing of supraglacial lakes in Greenland. *The Cryosphere Discussions* **12**, 3045–3065. doi: 10.5194/tc-12-3045-2018

Williamson AG, Willis IC, Arnold NS and Banwell AF (2018b) Controls on rapid supraglacial lake drainage in West Greenland: an Exploratory Data Analysis approach. *Journal of Glaciology* **64**(244), 208–226. doi: 10.1017/jog.2018.8